Scilight

Environmental and Microbial Technology

https://www.sciltp.com/journals/emt

Supplementary Materials

Microenvironmental Engineering of a Solid-State Electrolyte Reactor for Efficient Microbial Electrosynthesis of Acetate from CO_2

Na Chu [1,†], Xiaobing Wu [2,†], Weihong Zheng [2], Yanwei Luo [2], Hang Lin [2], Bingjie Sun [2], Huilin Chen [2], Chenghao Xu [2], Yan Wang [2], Xintong Xu [2], Jiping Tang [2,*], Yaoxing Liu [1] and Yong Jiang [2,*]

[1] Fujian Key Laboratory of Pollution Control and Resource Reuse, College of Environmental and Resource Sciences, Fujian Normal University, Fuzhou 350117, China
[2] Fujian Provincial Key Laboratory of Soil Environmental Health and Regulation, College of Resources and Environment, Fujian Agriculture and Forestry University, Fuzhou 350002, China
* Correspondence: jpt80027@foxmail.com (J.T.); jiangyongchange@163.com or jiangyongchange@fafu.edu.cn (Y.J.)
† These authors contributed equally to this work.

How To Cite: Chu, N.; Wu, X.; Zheng, W.; et al. Microenvironmental Engineering of a Solid-State Electrolyte Reactor for Efficient Microbial Electrosynthesis of Acetate from CO_2. *Environmental and Microbial Technology* **2026**, *1*(1), 11. https://doi.org/10.53941/emt.2026.100011

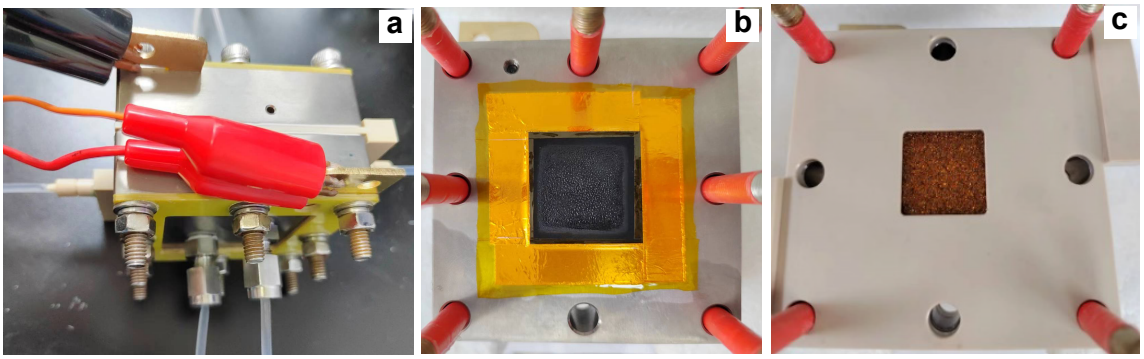

Figure S1. Three-chamber solid electrolyte reactor. (**a**) Photograph and (**b**) GDE and (**c**) middle chamber.

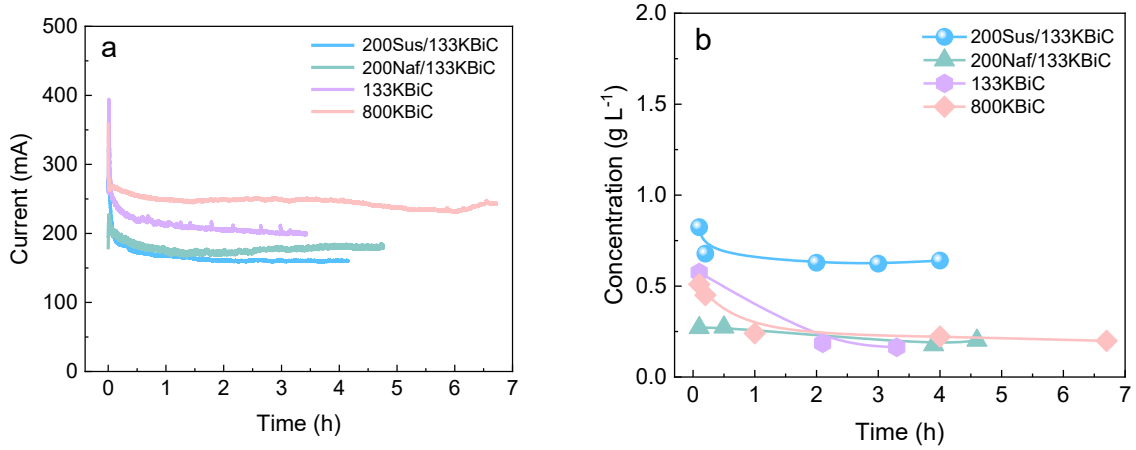

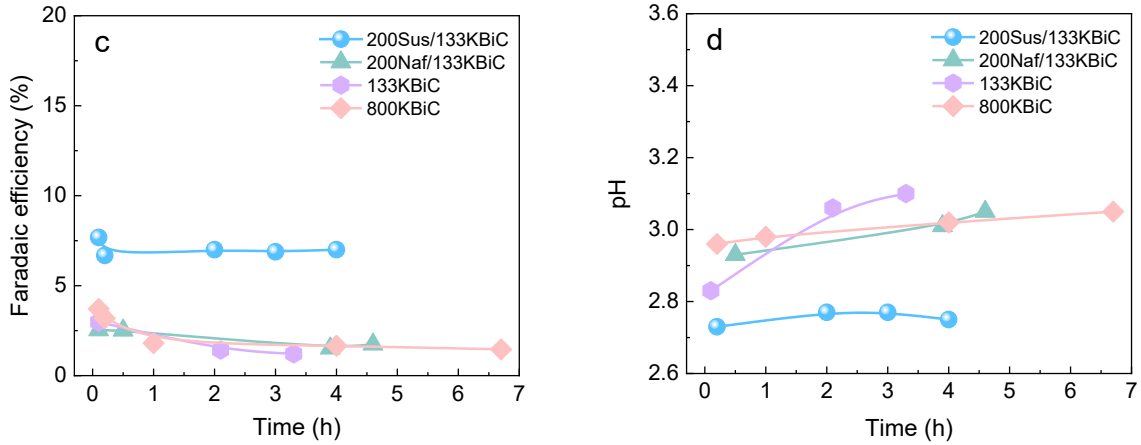

Figure S2. The performance of GDE prepared using method 1. (**a**) Current; (**b**) formate concentration; (**c**) Faradic efficiency and (**d**) pH.

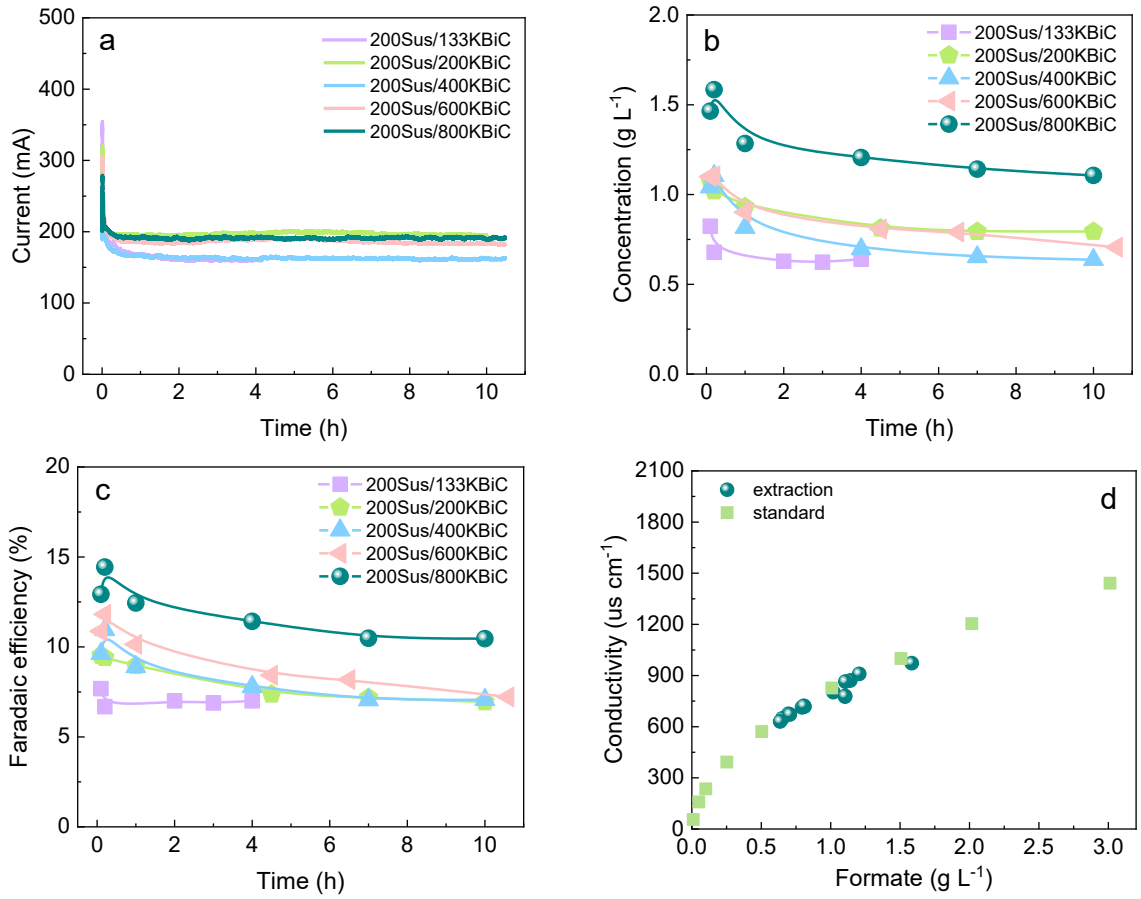

Figure S3. Potassium concentration of GDE prepared using method 1 was optimized. (**a**) Current; (**b**) formate concentration; (**c**) Faradic efficiency and (**d**) conductivity.

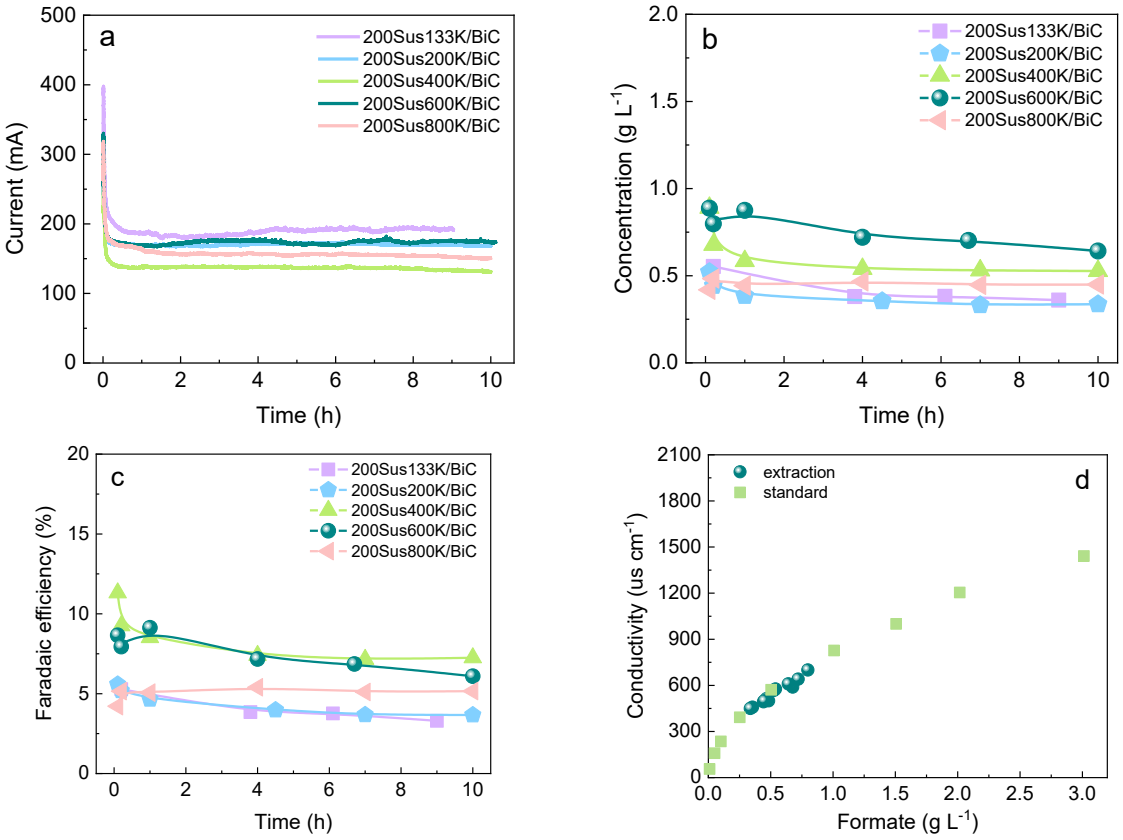

Figure S4. The performance of GDE prepared using method 2. (**a**) current; (**b**) formate concentration; (**c**) Faradic efficiency and (**d**) conductivity.

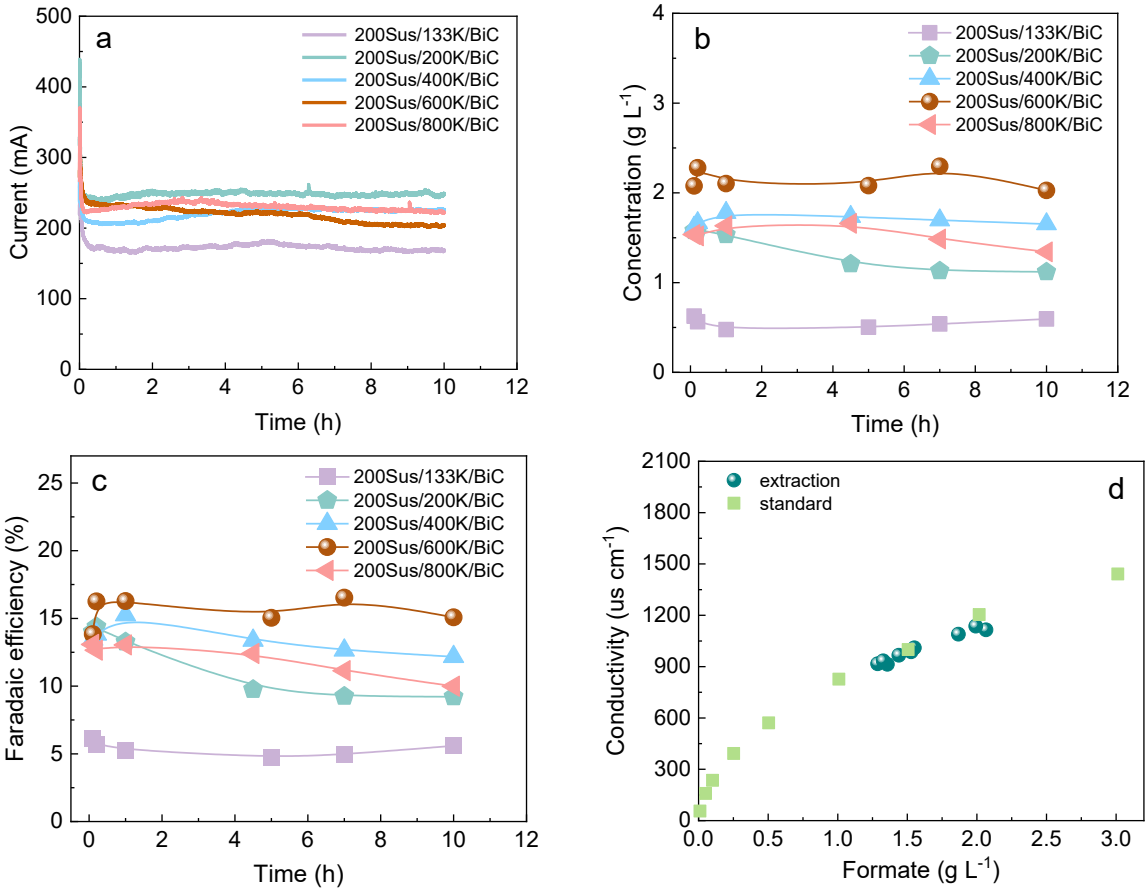

Figure S5. The performance of GDE prepared using method 3. (**a**) current; (**b**) formate concentration; (**c**) Faradic efficiency and (**d**) conductivity.

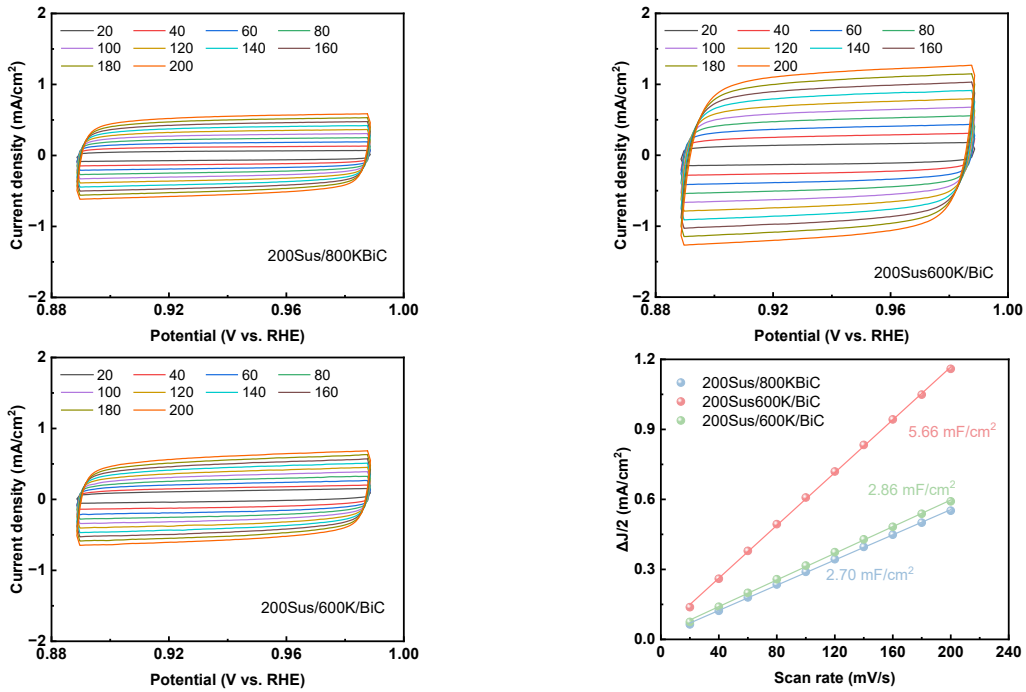

Figure S6. CV of GDE prepared with: (**a**) Method 1; (**b**) Method 2; (**c**) Method 3 and (**d**) Calculation of double-layer capacitance (C_{dl}) from CV curves.

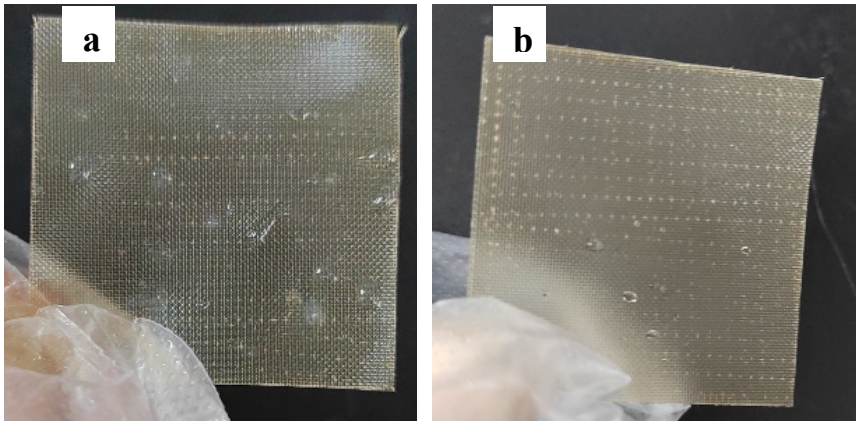

Figure S7. Photographs of the porous AEM, prepared by applying (**a**) a single pass (porous-once) or (**b**) two passes (porous-twice) of the needle roller on the Fumasep membrane.

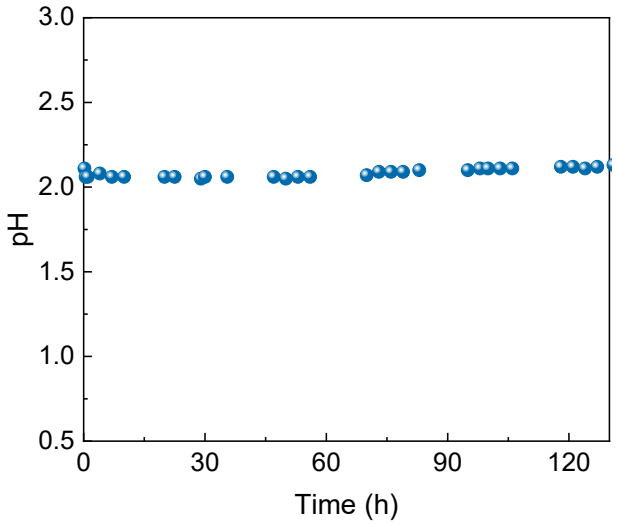

Figure S8. The pH of pure formic acid solution collected from the solid electrolyte reactor free of prefabricated AEM during continuous operation.

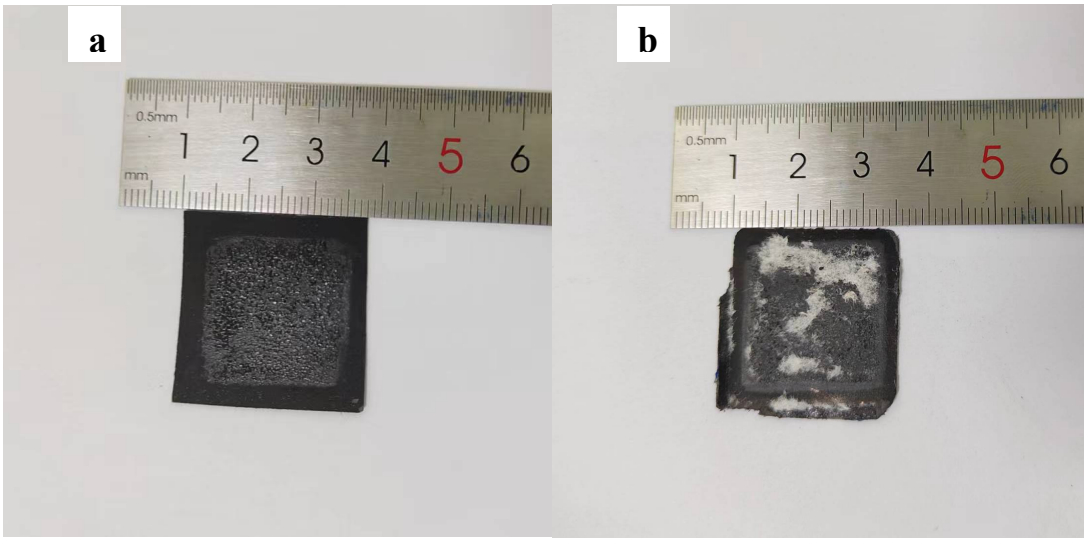

Figure S9. Photographs of the cation-infused sandwich-structured GDE: (**a**) pristine and (**b**) after long-term continuous operation with some filter paper fragments adhering to the surface.

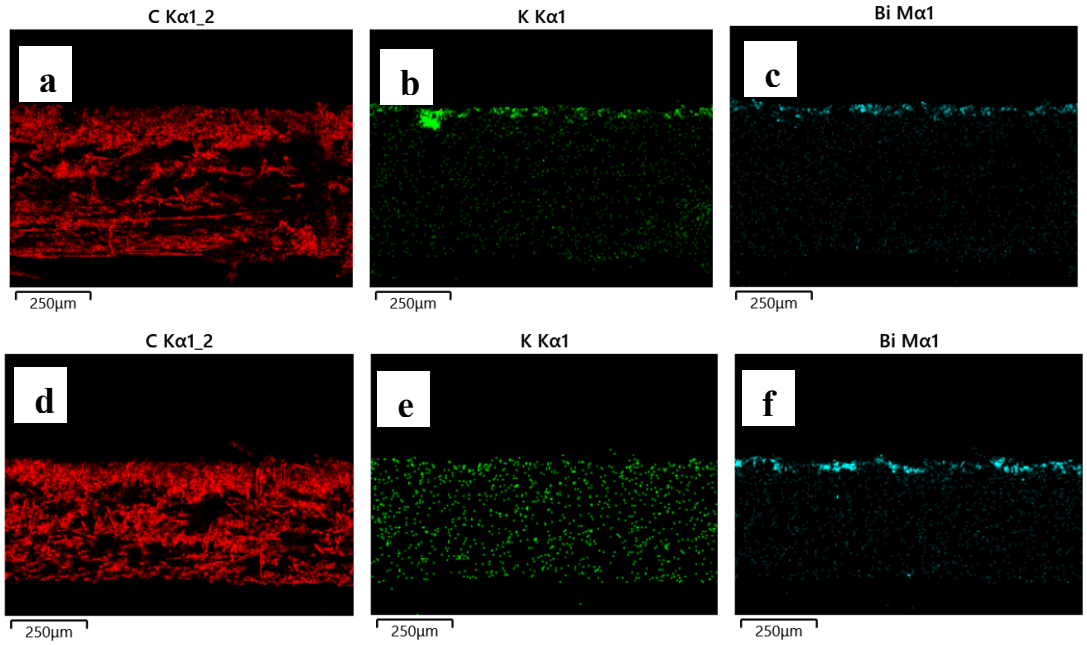

Figure S10. Cross-sectional EDS elemental mapping of (**a**–**c**) pristine and (**d**–**f**) after long-term continuous operation.

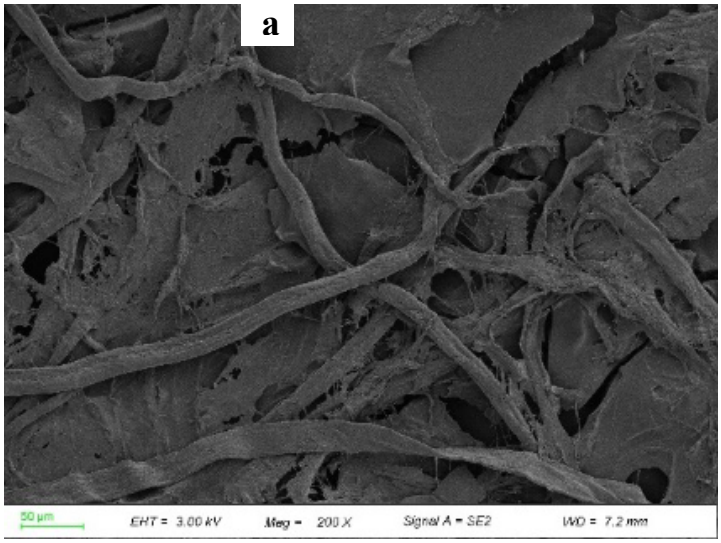

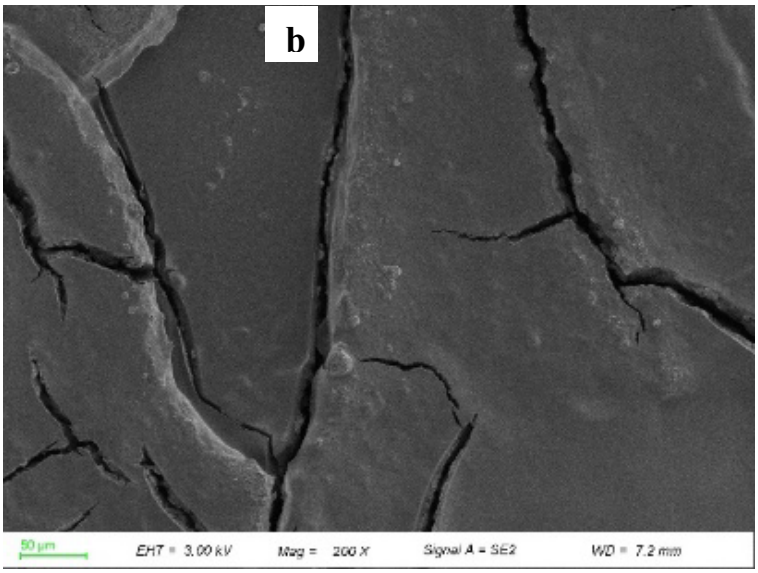

Figure S11. SEM of the cation-infused sandwich-structured GDE: (**a**) pristine and (**b**) after long-term continuous operation.

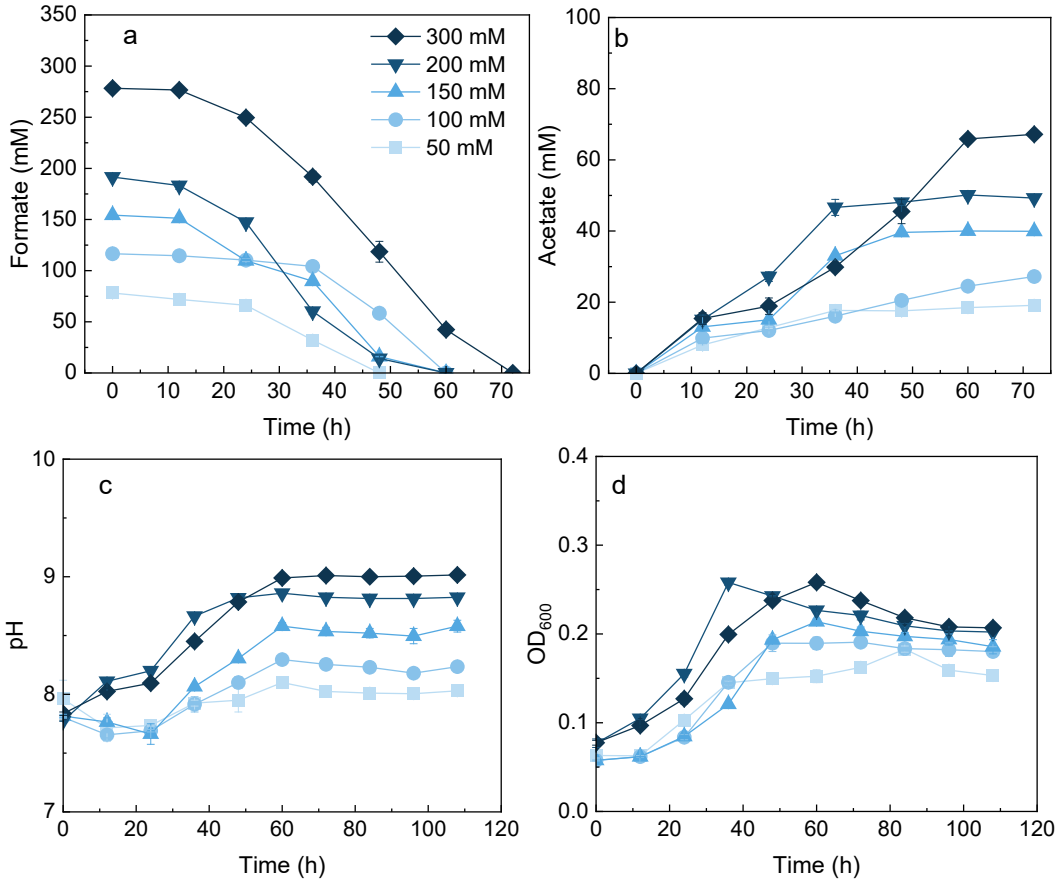

Figure S12. The effect of initial formate concentration on the acetogenesis performance of *A. woodii*. Key performance indicators monitored include: (**a**) formate consumption; (**b**) acetate production; (**c**) medium pH; and (**d**) bacterial growth (OD600).

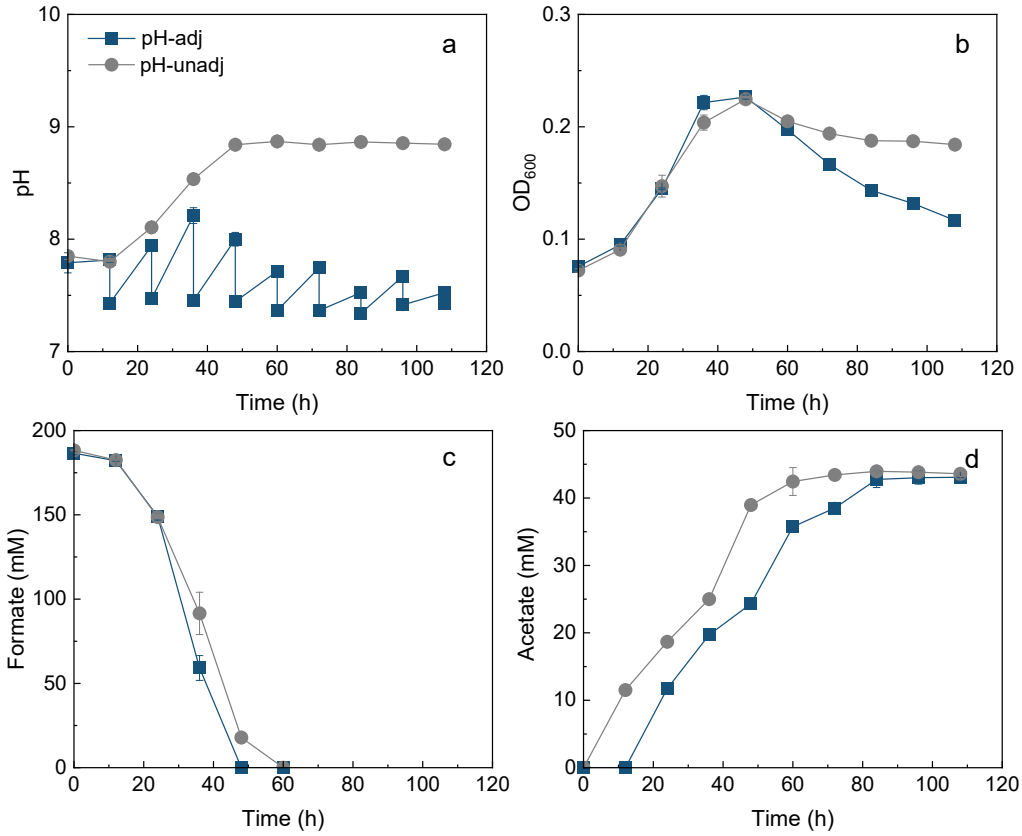

Figure S13. During formate conversion using *A. woodii*, the pH was maintained below 8 by the addition of HCl. The key performance indicators monitored were: (**a**) formate consumption; (**b**) acetate production; (**c**) medium pH, and (**d**) bacterial growth (OD600).

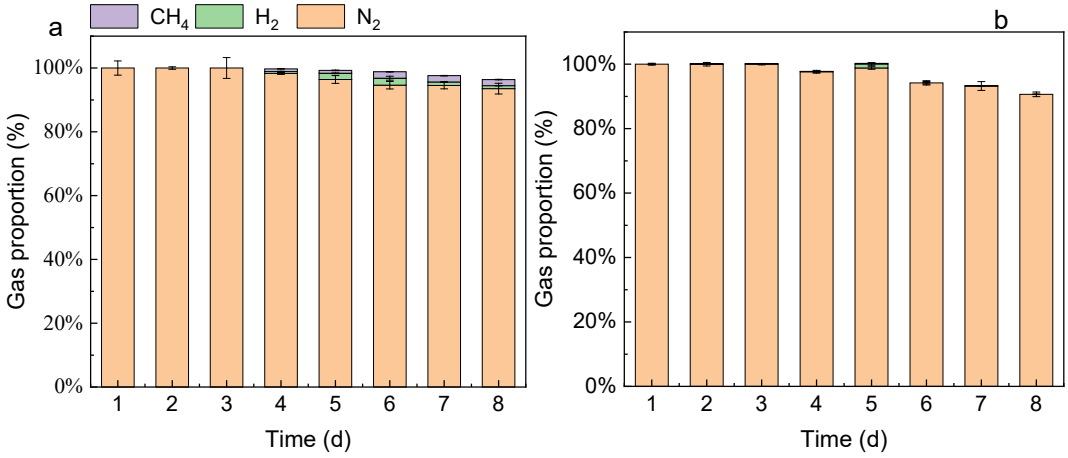

Figure S14. The enriched mixed culture for formate conversion was supplemented with 1× (2-BES X1) or 2× (2-BES X2) concentration of 2-bromoethanesulfonate: (**a**) Gas proportion in the 2-BES X1 group and (**b**) Gas proportion in the 2-BES X2 group.

Table S1. Abbreviations and full names of GDE corresponding to preparation methods.

Abbreviation	Full name
133KBiC	Bi+C+133 μL 0.15 M KOH/39BB GDL
800KBiC	Bi+C+800 μL 0.15 M KOH/39BB GDL
200Naf/133KBiC	200 μL 5%Nafion/Bi+C+133 μL 0.15 M KOH/39BB GDL
200Sus/133KBiC	200 μL 5%Sustainion/Bi+C+133 μL 0.15 M KOH/39BB GDL
200Sus/200KBiC	200 μL 5%Sustainion/Bi+C+200 μL 0.15 M KOH/39BB GDL
200Sus/400KBiC	200 μL 5%Sustainion/Bi+C+400 μL 0.15 M KOH/39BB GDL
200Sus/600KBiC	200 μL 5%Sustainion/Bi+C+600 μL 0.15 M KOH/39BB GDL
200Sus/800KBiC	200 μL 5%Sustainion/Bi+C+800 μL 0.15 M KOH/39BB GDL
200Sus133K/BiC	200 μL 5%Sustainion+133 μL 0.15 M KOH/Bi+C/39BB GDL

Table S1. *Cont*.

Abbreviation	Full name
200Sus200K/BiC	200 μL 5%Sustainion+200 μL 0.15 M KOH/Bi+C/39BB GDL
200Sus400K/BiC	200 μL 5%Sustainion+400 μL 0.15 M KOH/Bi+C/39BB GDL
200Sus600K/BiC	200 μL 5%Sustainion+600 μL 0.15 M KOH/Bi+C/39BB GDL
200Sus800K/BiC	200 μL 5%Sustainion+800 μL 0.15 M KOH/Bi+C/39BB GDL
200Sus/133K/BiC	200 μL 5%Sustainion/133 μL 0.15 M KOH/Bi+C/39BB GDL
200Sus/200K/BiC	200 μL5%Sustainion/200 μL 0.15 M KOH/Bi+C/39BB GDL
200Sus/400K/BiC	200 μL 5%Sustainion/400 μL 0.15 M KOH/Bi+C/39BB GDL
200Sus/600K/BiC	200 μL 5%Sustainion/600 μL 0.15 M KOH/Bi+C/39BB GDL
200Sus/800K/BiC	200 μL 5%Sustainion/800 μL 0.15 M KOH/Bi+C/39BB GDL

Table S2. Metal content of the collected formic acid solution at 0.5, 4.5 and 9.5 h during operation using GDE papered with different methods (Method 1, Method 2, and Method 3).

	Cu (mg L^{-1})	Fe (mg L^{-1})	K (mg L^{-1})	Na (mg L^{-1})	Bi (mg L^{-1})	Ag (mg L^{-1})
Method 1-0.5	0.00	0.01	1.94	0.00	0.02	0.00
Method 1-4.5	0.00	0.00	1.90	0.00	0.00	0.00
Method 1-9.5	0.00	0.01	1.54	0.00	0.03	0.00
Method 2-0.5	0.01	0.02	10.28	0.16	0.12	0.00
Method 2-4.5	0.00	0.01	12.33	0.63	0.08	0.00
Method 2-9.5	0.00	0.01	6.73	0.18	0.08	0.00
Method 3-0.5	0.00	0.01	9.71	0.00	0.04	0.00
Method 3-4.5	0.00	0.01	5.69	0.00	0.01	0.00
Method 3-9.5	0.00	0.00	3.70	0.00	0.02	0.00

Table S3. Metal content in formic acid solution after over 130 h of continuous operation with 200Sus/600K/BiC at 240 mA.

	Cu (mg L^{-1})	Fe (mg L^{-1})	K (mg L^{-1})	Na (mg L^{-1})	Bi (mg L^{-1})	Ag (mg L^{-1})
Concentration	0.000	0.003	0.098	0.000	0.000	0.000

Table S4. Cross-sectional EDS mapping analysis of different GDE samples.

Samples	Element	Line type	Weight %	Weight % Sigma	Atomic %
Pristine	C	K series	97.93	0.22	99.68
	K	K series	0.80	0.06	0.25
	Bi	M series	1.27	0.21	0.07
Used	C	K series	97.92	0.21	99.87
	K	K series	0.03	0.05	0.01
	Bi	M series	2.05	0.20	0.12

Table S5. Performance comparation of pure formic acid production from SSE reactors.

Catalyst	AEM	Stability (h)	Current Density (mA cm^{-2})	Concentration (M)	FE (%)	Ref.
Commercial Bi	w/o	202	60	0.11	40	This study
Bi microsheets	Sustainion X37–50 Grade 60	110	160	0.13	80	[1]
Bi_2O_3 nanosheets	Sustainion X37-50 Grade 60	43	56	0.1	80	[2]
Bi_2S_3-derived	Sustainion X37-50 Grade RT	280	100	0.3	90	[3]
SiC/SnBi	Sustainion-FA™	12	100	0.41	83	[4]
In_2O_3@C	Sustainion X37-50	3	30	0.12	80	[5]
Single-atom Pb_1Cu	Dioxide Materials	180	100	0.1	85	[6]
nBuLi-treated Bi	Dioxide Materials	100	30	0.1	78	[7]
2D-Bi	Dioxide Materials	100	30	0.11	80	[8]
Bi nanowires	Sustainion X37-50 Grade 60	120	45	1.1	82.2	[9]
CuBi-R	QAPPT	200	100	0.7	85	[10]
Bi-HHTP	Alkymer alkaline polymer	30	~80	0.2	90	[11]
defects-enriched Bi	QAPPT	24	N.A.	0.2	~90	[12]
CuO/Cu NSO_4/CN	Sustainion X37-50 Grade 60	N.A.	~18	0.1	87.9	[13]
asymmetrically stretched InO_5S	N.A.	10	20	N.A.	N.A.	[14]
$BiSbO_x$/C	Sustainion X37-50 Grade 60	13.3	50	N.A.	88.5	[15]
BS/VC hybrid	Dioxide Materials	120	50	N.A.	80	[16]
Ag/Sn–SnO_2 NSs	N.A.	200	100	~0.1	90	[17]
Bi−Cu/HMCS	Sustainion X37-50 Grade FA	18	100	0.2	N.A.	[18]
InNCN	N.A.	160	124.7	N.A.	80.9	[19]

References

1. Zhang, Y.; Zhang, R.; Chen, F.; et al. Mass-Transfer-Enhanced Hydrophobic Bi Microsheets for Highly Efficient Electroreduction of CO_2 to Pure Formate in a Wide Potential Window. *Appl. Catal. B Environ.* **2023**, *322*, 122127.
2. Tan, Z.; Zhang, J.; Yang, Y.; et al. Continuous Production of Formic Acid Solution from Electrocatalytic CO_2 Reduction Using Mesoporous Bi_2O_3 Nanosheets as Catalyst. *CCS Chem.* **2024**, *6*, 100–109.
3. Lin, L.; He, X.; Zhang, X.G.; et al. A Nanocomposite of Bismuth Clusters and $Bi_2O_2CO_3$ Sheets for Highly Efficient Electrocatalytic Reduction of CO_2 to Formate. *Angew. Chem. Int. Ed.* **2023**, *62*, e202214959.
4. Li, L.; Liu, Z.; Yu, X.; et al. Achieving High Single-Pass Carbon Conversion Efficiencies in Durable CO_2 Electroreduction in Strong Acids via Electrode Structure Engineering. *Angew. Chem. Int. Ed.* **2023**, *62*, e202300226.
5. Wang, Z.; Zhou, Y.; Liu, D.; et al. Carbon-Confined Indium Oxides for Efficient Carbon Dioxide Reduction in a Solid-State Electrolyte Flow Cell. *Angew. Chem. Int. Ed.* **2022**, *61*, e202200552.
6. Zheng, T.; Liu, C.; Guo, C.; et al. Copper-Catalysed Exclusive CO_2 to Pure Formic Acid Conversion via Single-Atom Alloying. *Nat. Nanotechnol.* **2021**, *16*, 1386–1393.
7. Fan, L.; Xia, C.; Zhu, P.; et al. Electrochemical CO_2 Reduction to High-Concentration Pure Formic Acid Solutions in an All-Solid-State Reactor. *Nat. Commun.* **2020**, *11*, 3633.
8. Xia, C.; Zhu, P.; Jiang, Q.; et al. Continuous Production of Pure Liquid Fuel Solutions via Electrocatalytic CO_2 Reduction Using Solid-Electrolyte Devices. *Nat. Energy* **2019**, *4*, 776–785.
9. Liu, G.; Zhong, Y.; Liu, Z.; et al. Solar-Driven Sugar Production Directly from CO_2 via a Customizable Electrocatalytic-Biocatalytic Flow System. *Nat. Commun.* **2024**, *15*, 2636.
10. Zhang, G.; Tan, B.; Mok, D.H.; et al. Electrifying HCOOH Synthesis from CO_2 Building Blocks over Cu-Bi Nanorod Arrays. *Proc. Natl. Acad. Sci. USA* **2024**, *121*, e2400898121.
11. Zhao, Z.H.; Huang, J.R.; Huang, D.S.; et al. Efficient Capture and Electroreduction of Dilute CO_2 into Highly Pure and Concentrated Formic Acid Aqueous Solution. *J. Am. Chem. Soc.* **2024**, *146*, 14349–14356.
12. Zhang, G.; Ji, N.; Lyu, S.; et al. Artificial Synthesis of Polyesters at Ambient Condition via Consecutive CO_2 Electrolysis and Fermentation. *Nano Res.* **2024**, *17*, 6016–6025.
13. Yuan, C.Y.; Feng, L.; Qin, X.; et al. Constructing Metal(II)-Sulfate Site Catalysts toward Low Overpotential Carbon Dioxide Electroreduction to Fuel Chemicals. *Angew. Chem. Int. Ed.* **2024**, *63*, e202405255.
14. Sun, Y.; Dai, L.; Sui, N.L.D.; et al. Direct Parallel Electrosynthesis of High-Value Chemicals from Atmospheric Components on Symmetry-Breaking Indium Sites. *Proc. Natl. Acad. Sci. USA* **2024**, *121*, e2409620121.
15. Li, X.; Wang, J.H.; Yuan, C.Y.; et al. A Unique Amorphous Porous $BiSbO_x$ Nanotube with Abundant Unsaturated Sb-Stabilized BiO_{8-x} Sites for Efficient CO_2 Electroreduction in a Wide Potential Window. *Adv. Funct. Mater.* **2024**, *34*, 2402220.
16. Zhu, J.; Li, J.; Lu, R.; et al. Surface Passivation for Highly Active, Selective, Stable, and Scalable CO_2 Electroreduction. *Nat. Commun.* **2023**, *14*, 4670.
17. Zhang, M.; Cao, A.; Xiang, Y.; et al. Strongly Coupled Ag/Sn–SnO_2 Nanosheets toward CO_2 Electroreduction to Pure HCOOH Solutions at Ampere-Level Current. *Nano-Micro Lett.* **2023**, *16*, 50.
18. Wang, X.; Zhou, M.; Wang, M.; et al. Copper-Bridge-Enhanced p-Band Center Modulation of Carbon-Bismuth Heterojunction for CO_2 Electroreduction. *Nano Lett.* **2023**, *23*, 10946–10954.
19. Jia, B.; Chen, Z.; Li, C.; et al. Indium Cyanamide for Industrial-Grade CO_2 Electroreduction to Formic Acid. *J. Am. Chem. Soc.* **2023**, *145*, 14101–14111.